Polymer 50 (2009) 4602–4611

Contents lists available at ScienceDirect

Polymer

journal homepage: www.elsevier.com/locate/polymer

Hole-limiting conductive vinyl copolymers for AlQ_3-based OLED applications

Tik H. Lee, K.M. Lai, Louis M. Leung*

Department of Chemistry and Centre for Advanced Luminescence Materials (CALM), Hong Kong Baptist University, Kowloon, Hong Kong SAR, China

ARTICLE INFO

Article history:
Received 6 March 2009
Received in revised form
16 July 2009
Accepted 22 July 2009
Available online 25 July 2009

Keywords:
N-(4-Methoxyphenyl)-*N*-(4-vinylphenyl)naphthalen-1-amine
2-Phenyl-5-(4-vinylphenyl)-1,3,4-oxadiazole
Charge-balance
OLED

ABSTRACT

A series of soluble conductive vinyl copolymers containing a hole-transporting *N*-(4-methoxyphenyl)-*N*-phenylnaphthalen-1-amine (MeONPA) moiety and an electron-transporting/hole-blocking 2,5-diphenyl-1,3,4-oxadiazole (OXA) moiety at different composition ratios were synthesized and characterized. The copolymers were applied as the hole-transporting layer (HTL) for a series of heterojunction Organic Light-emitting Diodes (OLEDs) employing the commonly used green emitter tris(8-hydroxyquinolinato)aluminum (AlQ_3) as the electron-transporting layer. AlQ_3 is known to have inferior electron mobility compared to most typical hole-transporting materials. As a result, oxidative degradation of the AlQ_3 emitters caused by the excessive holes accumulated at the interface led to deterioration of the device over time. From the measurement of hole current only devices using electron blocking gold as cathode (ITO/PEDOT:PSS/copolymer/Au), it was found that the hole current for the copolymers reduced as the OXA composition increased. Optimum performance for the AlQ_3-based OLED (ITO/PEDOT:PSS/copolymer/AlQ_3/Ca/Al) was achieved for a 82/18 (molar ratio) (MeONPA/OXA) copolymer. The maximum current efficiency and luminance were 4.2 cd/A and ca 24,000 cd/m^2 respectively for the charge-balanced copolymer compared to 3.5 cd/A and 6600 cd/m^2 for similar device employing a homopolymer P(MeONPA) as the HTL.

1. Introduction

Since the discovery of heterojunction tris(8-hydroxyquinolinato)-aluminum (AlQ_3)-based OLEDs by the Kodak's group in 1987 [1], AlQ_3 remained as one of the most important electron-transporting materials for the fabrication of OLED display devices. Heterojunction OLED having superior efficiency due to exciton formation was confined at or near the interface between the two organic layers (hole and electron-transporting layers) with opposite charge transporting properties. AlQ_3 is a green emitting fluorescent dye ($\lambda_{max} = 520$ nm) and can be used as an electron-transporting layer or a host for other bluish-green to red fluorescent dyes [2]. Its ease of preparation, excellent thermal stability ($T_g = 172$ °C) [3] and formation of uniform thin film using vacuum deposition technique [4] are material properties highly sought for small molecule-based OLEDs. AlQ_3, however, has electron mobility (10^{-6}–10^{-7} cm^2/V s) [5] one to two orders lower than the most hole-transporting small molecules commonly used for OLED (e.g. TPD and NPB have hole mobility in the range 1×10^{-3} cm^2/V s). The unbalanced hole and electron currents not only reduced the OLED efficiency but also caused the formation of degradative cationic AlQ_3^+ species [3,6–11]. These cationic species are fluorescence quenchers and trap for charge as well. As a result, long-term performance of the device gradually deteriorated.

Several approaches have been attempted to reduce the hole current for AlQ_3-based OLEDs. They are: (i) doping the hole-transporting layer (HTL) with rubrene or a salt-containing polymer [12,13]; (ii) inserting a hole-retarding buffer layer between the ITO anode and the HTL [14–16]; and (iii) using hole-transporting material (HTM) with moderate hole mobility [17]. It is expected that as the hole current is impeded, the concentration of holes at the HTL/AlQ_3 interface would be reduced. As the HOMO for most HTL is higher than the HOMO for the ETL, leaking of holes into the AlQ_3 layer has been suggested the cause for the formation of the cationic AlQ_3^+ species. Recently, Thomas et al. incorporated some electron-deficient segments into an arylamine moiety for the preparation of various bipolar small molecules such as quinoxaline-triarylamine and oxadiazole-triarylamine for use as HTL for AlQ_3-based heterojunction devices [18–21]. Their results also indicated a hole-impeding effect as non-emissive wide band-gap hole-blocking elements were incorporated into the HTL.

Vinyl conductive copolymer has the advantage over traditional main-chain conjugated conductive polymer that they are soluble even at high molecular weight and can be easily solution processed into thin film with excellent mechanical properties. Vinyl copolymers containing triphenylamine, diphenyl-1,3,4-oxadiazole and

* Corresponding author. Tel.: +852 3411 7073; fax: +852 3411 7348.
E-mail address: s20974@hkbu.edu.hk (L.M. Leung).

0032-3861/$ – see front matter © 2009 Elsevier Ltd. All rights reserved.
doi:10.1016/j.polymer.2009.07.034

diphenylqunioxaline has been reported as a host for fluorescent additive [22a]. Side-chain copolymers containing boron emitter and high emission efficiency phosphorescent dye have also been reported for POLED [22b,c]. We have previously reported mobility measurement for some *N*-phenyl-*N*-phenylnaphthalen-1-amine (NPA) hole-transporting model compounds with different substituted side groups (e.g. H-NPA, MeO-NPA, F-NPA) [23] and their respective vinyl polymers [24]. The vinyl polymers were found to be soluble in most common organic solvents despite their high molecular weight (MW). They have high glass transition temperature ($T_{g\ midpoint} = 161\ ^{\circ}C$ for poly(H-NPA)) and good hole mobility ($0.5–2 \times 10^{-4}\ cm^2/V\,s$) as well. In this manuscript, we shall report the synthesis of a series of hole-limiting vinyl copolymers via free-radical copolymerization of *N*-(4-methoxyphenyl)-*N*-(4-vinylphenyl)-naphthalen-1-amine (vMeONPA) and 2-phenyl-5-(4-vinylphenyl)-1,3,4-oxadiazole (vOXA) [25], and their applications as hole-limiting HTL for OLEDs [26,27]. The OXA moiety is a well-known electron-transporting material but due to its wide band-gap (or low-lying HOMO) is also a hole-blocking material. The hole-limiting copolymers have several advantages compared to their small molecules analogs. They are such as (i) the hole current for the copolymer can be tailored simply by changing the MeONPA/OXA monomer feed ratios in order to match the electron current of the ETL; (ii) the highly soluble vinyl copolymers can be solution or spin coat on large surface area under atmospheric conditions; and (iii) the copolymers have better thermal stability than most of the small molecule-based HTM. Blending a hole-transporting polymer with hole-blocking small molecules (guest–host system) or formation of alloys between hole-transporting and hole-blocking polymers could lead to microphase segregation eventually, especially during high current device operation condition, whereas a homogeneous copolymer would not [27,28].

2. Experimental section

2.1. General

All reactions were carried out under nitrogen atmosphere using standard Schlenk techniques unless specified otherwise. Analytical grade solvents were purified by distillation over appropriate drying agents under an inert nitrogen atmosphere prior to use. All reagents and chemicals, unless otherwise stated, were purchased from commercial sources and used without further purification. The positive-ion fast atom bombardment (FAB) mass spectra were recorded in *m*-nitrobenzyl alcohol matrices in a Finnegan-MAT SSQ710 mass spectrometer. Infrared spectra were recorded on a Nicolet Magna 550 Series II FTIR spectrometer, using KBr pellets for solid state spectroscopy. NMR spectra were measured using deuterated solvent as the lock and reference on a JEOL JNM-EX270 FT NMR system or a Varian INOVA 400 MHz FT NMR spectrometer. ^1H NMR chemical shifts were quoted relative to Me_4Si. Electronic absorption spectra were obtained with a Hewlett Packard 8453 spectrometer. Solution photoluminescence measurements were obtained by an LS50B fluorescent spectrometer. Cyclic voltammetry measurements were performed on a BAS CV-50W electrochemical analyzer. All CV measurements were carried out at room temperature with a conventional three-electrode configuration consisting a platinum working and counter electrodes and a Ag/AgCl reference electrode. The supporting electrolyte was 0.1 M tetrabutylammonium hexafluorophosphate ($[Bu_4N]PF_6$) dissolved in ACN and each measurement was calibrated with an internal standard, ferrocene/ferrocenium (Fc/Fc^+) redox couple. The molecular weights of the polymers were determined by GPC (HP 1050 series HPLC with visible wavelength and fluorescent detectors) using polystyrene MW standards. Thermal analyses were performed on a Perkin–Elmer Pyris Diamond DSC and a Perkin–Elmer TGA6 thermal analyzers.

2.1.1. *N*-(4-Methoxyphenyl)-*N*-phenylnaphthalen-1-amine (MeONPA)

N-Phenylnaphthalen-1-amine (10.0 g, 46.0 mmol), 4-iodoanisole (12.9 g, 52 mmol), CuI (0.9 g, 4.6 mmol) and 1,10-phenanthroline (0.80 g, 4.6 mmol) were dissolved and stirred with overhead stirrer in 100 mL *p*-xylene under nitrogen pressure. The mixture was heated to reflux. Potassium hydroxide (21.0 g, 322.0 mmol) was added. The mixture was further refluxed for another 6 h. The product was neutralized with acetic acid and extracted with toluene. The solution passed through silica gel and the yellowish solution was concentrated under reduced pressure. Pale yellow crystals were obtained at 75% yield. ^1H NMR ($CDCl_3$): $\delta = 3.74$ (s, 3H), 6.75–6.83 (m, 4H), 7.05–7.15 (m, 4H), 7.22–7.48 (m, 6H), 7.69–7.72 (d, $J = 8.1$ Hz, 1H), 7.83–7.86 (d, $J = 8.1$ Hz, 2H), 7.93–7.96 (d, $J = 8.1$, 1H). MS (FAB): m/z 325 (M^+). Elemental Anal. Calcd for $C_{23}H_{19}NO$: C, 84.89%; H, 5.89%; N, 4.30%; O, 4.92%. Found: C, 84.10%; H, 5.71%; N, 4.13%.

2.1.2. 4-((4-Methoxyphenyl)(naphthalen-1-yl)amino)benzaldehyde (MeONPA-CHO)

To a two necked round-bottom flask, MeONPA (2.0 g, 6.2 mmol) was dissolved in DMF with 1 equivalent $POCl_3$. The reaction mixture was heated to 65 °C and stirred overnight. The mixture was then poured into ice water and neutralized by Na_2CO_3. It was extracted with dichloromethane and purified by column chromatography using hexane/dichloromethane (3:7 v/v). The yield was approx. 90%. ^1H ($CDCl_3$): $\delta = 3.75$ (s, 3H), 6.87 (d, $J = 8.1$ Hz, 2H), 7.08–7.13 (m, 1H), 7.21–7.53 (m, 9H), 7.63 (d, $J = 8.1$ Hz, 2H), 7.82–7.92 (m, 3H), 9.76 (s, 1H). MS (FAB): m/z 353 (M^+).

2.1.3. *N*-(4-Methoxyphenyl)-*N*-(4-vinylphenyl)naphthalen-1-amine (vMeONPA)

To a 250 mL round-bottom flask, methyl triphenyl phosphonium (2.1 g, 51.0 mmol) was dissolved in 50 mL freshly distillated THF. Potassium *tert*-butyl oxide (0.6 g, 51.0 mmol) was added and stirred for 30 min. A reddish-yellow solution resulted. 4-((4-Methoxyphenyl)(naphthalen-1-yl)amino)benzaldehyde (1.5 g, 42.0 mmol) dissolved in THF was added and the solution turned to a white-opaque color. The mixture was stirred at room temperature (r.t.) for another 3 h. Finally a yellowish solution was obtained and completion of the reaction was indicated by TLC. For extraction, the mixture was first neutralized by HCl and then extracted by dichloromethane. Higher purity can be achieved by column chromatography using hexane. A colorless liquid was obtained. White crystals were formed at −4 °C. The yield was approx. 90%. ^1H ($CDCl_3$): $\delta = 7.93$ (d, $J = 8.1$ Hz, 1H), 7.86 (d, $J = 8.1$ Hz, 1H), 7.73 (d, $J = 8.1$ Hz, 1H), 7.41–7.47 (t, $J = 8.1$ Hz, 2H), 7.32–7.37 (t, $J = 7.6$ Hz, 1H), 7.08 (d, $J = 8.1$ Hz, 2H), 7.11 (d, $J = 8.1$ Hz, 2H), 7.27 (d, $J = 8.1$ Hz, 1H), 6.79 (d, $J = 8.1$ Hz, 4H), 6.56–6.66 (dd, $J = 10.8$ and 17.5 Hz, 1H), 5.55 (d, $J = 17.5$ Hz, 1H), 5.07 (d, $J = 10.8$ Hz, 1H), 3.77 (s, 3H). MS (FAB): m/z 351 (M^+).

2.1.4. 4-(5-Phenyl-1,3,4-oxadiazol-2-yl)benzaldehyde (OXA-CHO)

4-Formylbenzoyl chloride (5.6 g, 37.0 mmol) and 5-phenyl-2*H*-tetrazole (5.0 g, 34.0 mmol) were dissolved in 200 mL pyridine. The solution was refluxed for 24 h. The solvent was evaporated under reduced pressure and the residues were washed with ethanol several times. A white solid resulted in 85% yield. ^1H ($CDCl_3$): $\delta = 7.53–7.55$ (m, 3H), 8.03 (d, $J = 8.1$ Hz, 2H), 8.12–8.15 (m, 2H), 8.30 (d, $J = 8.1$ Hz, 2H), 10.08 (s, 1H). MS (FAB): m/z 351 ($M^+ + 1$). Elemental Anal. Calcd. for $C_{15}H_{10}N_2O_2$: C, 71.99%; H, 4.03%; N, 11.19%; O, 12.79%. Found: C, 72.22%; H, 4.00%; N, 12.92%.

2.1.5. 2-Phenyl-5-(4-vinylphenyl)-1,3,4-oxadiazole (vOXA)

To a 250 mL round-bottom flask, the ylide (5.1 g, 14.4 mmol) was dissolved in 50 mL freshly distillated THF. Potassium *tert*-butyl oxide (13.2 g, 13.2 mmol) was added and stirred for 30 min in an ice bath. A yellowish solution resulted. 4-(5-Phenyl-1,3,4-oxadiazol-2-yl)benzaldehyde (3.0 g, 14.4 mmol) dissolved in THF was then added. The mixture was stirred continuously until completion of reaction as indicated by TLC. For extraction, the mixture was first neutralized by HCl and then extracted by dichloromethane. Higher purity can be achieved by column chromatography using hexane. A colorless liquid was obtained. White crystals were formed at −4 °C at 80% yield. ^{1}H ($CDCl_3$): $\delta = 5.43$ (d, $J = 10.8$ Hz, 1H), 5.92 (d, $J = 17.5$ Hz, 1H), 6.75–6.86 (dd, $J = 10.8$ and 17.5 Hz, 1H), 7.56–7.61 (m, 5H), 8.12–8.19 (m, 4H). MS (FAB): m/z 249 ($M^+ + 1$). Elemental Anal. Calcd for $C_{16}H_{12}N_2O$: C, 77.40%; H, 4.87%; N, 11.28%; O, 6.44%. Found: C, 77.01%; H, 5.17%; N, 10.99%.

2.2. Free-radical polymerization

To a 10 mL one mouth glass apparatus charged with magnetic stirring bar, the respective vinyl compound(s) at different feed ratios (F_1 = molar percentage of MeONPA, F_2 = molar percentage of OXA, total feed ($F_1 + F_2$) = 1.1 mmol) and AIBN (3.6 mg, 0.02 mmol) were dissolved in 2 mL toluene freshly distillated from sodium metal. The reaction mixture was degassed by several freeze–pump–thaw cycles and then sealed off. The reaction mixture was stirred at 80 °C for 10 h. Finally, a yellowish gel resulted. The polymer gel was precipitated from excess acetone and re-dissolved in THF for a second re-precipitation yielding a pale yellowish powder. The compositions of the copolymer were determined by NMR and their FT-IR and NMR characteristics are listed below.

2.2.1. P(MeONPA)

FT-IR (KBr pellet): 1117–1280 cm^{-1} (C–N in aromatic amide). ^{1}H (CD_2Cl_2): $\delta = 6.49$–7.72 (aromatic H, 16H), 3.52 (MeO–H, 3H), 1.85 (aliphatic H), 1.48 (aliphatic H).

2.2.2. P(OXA)

FT-IR (KBr pellet): 962 cm^{-1} (C–O–C), 1073 cm^{-1} (C–O) and 1619 cm^{-1} (C═N). ^{1}H (CD_2Cl_2): $\delta = 6.62$–7.90 (aromatic H, 9H), 1.79 (aliphatic H), 1.28 (aliphatic H).

2.2.3. P(MeONPA-co-OXA), $F_1 = 0.95$

FT-IR (KBr pellet): 961 cm^{-1} (C–O–C), 1072 cm^{-1} (C–O), 1617 cm^{-1} (C═N) and 1237–1280 cm^{-1} (C–N in aromatic amide). ^{1}H ($CDCl_3$): $\delta = 6.49$–7.73 (aromatic H, 16.67H), 3.52 (MeO–H, 3H), 1.89 (aliphatic H), 1.47 (aliphatic H).

2.2.4. P(MeONPA-co-OXA), $F_1 = 0.85$

FT-IR (KBr pellet): 960 cm^{-1} (C–O–C), 1073 cm^{-1} (C–O), 1616 cm^{-1} (C═N) and 1236–1281 cm^{-1} (C–N in aromatic amide). ^{1}H (CD_2Cl_2): $\delta = 6.49$–7.73 (aromatic H, 17.98H), 3.50 (MeO–H, 3H), 1.88 (aliphatic H), 1.46 (aliphatic H).

2.2.5. P(MeONPA-co-OXA), $F_1 = 0.70$

FT-IR (KBr pellet): 958 cm^{-1} (C–O–C), 1071 cm^{-1} (C–O), 1615 cm^{-1} (C═N) and 1237–1281 cm^{-1} (C–N in aromatic amide). ^{1}H (CD_2Cl_2): $\delta = 6.49$–7.73 (aromatic H, 20.03H), 3.57 (MeO–H, 3H), 1.89 (aliphatic H), 1.48 (aliphatic H).

2.2.6. P(MeONPA-co-OXA), $F_1 = 0.50$

FT-IR (KBr pellet): 962 cm^{-1} (C–O–C), 1073 cm^{-1} (C–O), 1619 cm^{-1} (C═N) and 1238–1280 cm^{-1} (C–N in aromatic amide). ^{1}H (CD_2Cl_2): $\delta = 6.63$–7.90 (aromatic H, 26.17H), 3.52 (MeO–H, 3H), 1.85 (aliphatic H), 1.45 (aliphatic H).

2.2.7. P(MeONPA-co-OXA), $F_1 = 0.30$

FT-IR (KBr pellet): 959 cm^{-1} (C–O–C), 1073 cm^{-1} (C–O), 1616 cm^{-1} (C═N) and 1237–1281 cm^{-1} (C–N in aromatic amide). ^{1}H (CD_2Cl_2): $\delta = 6.65$–7.79 (aromatic H, 41.61H), 3.58 (MeO–H, 3H), 1.89 (aliphatic H), 1.56 (aliphatic H).

2.3. OLED devices fabrication

ITO glass with 30 ohm/square sheet resistance was cleansed by rubbing with industrial detergent and then heated in a bath containing Deconex. It was then washed with distilled water, ethanol and acetone sequentially in an ultrasonic bath for 10 min each. At the end, the ITO glass was exposed to UV–ozone treatment for 10 min in order to remove all residue organic contaminants. A 25 nm hole-injecting layer poly(ethylenedioxythiophene)/poly-(styrene sulfonic acid) (PEDOT:PSS) was spin cast (P6700 spin coating system) onto the ITO substrate. The 1:1.6 PEDOT:PSS aq. emulsion (Aldrich) was filtered with a 0.45 μm and then a 0.2 μm PVDF filter before use. The PEDOT coated ITO glass was dried in an oven at 150 °C for 10 min under nitrogen environment. The copolymers were dissolved in chlorobenzene to a concentration of 20 mg/mL. Prior to spin coating, the copolymer solutions were filtered using a PTFE filter with 0.45 μm pore size. The copolymer thin film was dried in an oven at 70 °C for 24 h under nitrogen and then 90 °C for another 24 h under vacuum. The film thickness of the copolymer was ca 100 nm. The film thickness was confirmed by a Tencor profilometer. For the heterojunction OLED devices, 60 nm of AlQ_3 was vacuum evaporated onto the HT copolymer at a deposition rate of 0.1 nm/s using a Denton Vacuum Evaporator DV-502V. The AlQ_3 was purified by train-sublimation before use. Thirty nm of calcium was vacuum deposited using a mask as the low work function cathode and then encapsulated with 100 nm of aluminum using an Edwards Auto 306 evaporator. The deposition rates were 0.2 nm/s and 1 nm/s for Ca and Al respectively. The active device area was about 0.0357 cm^2. The Current–Voltage–Luminance (I–V–L) and electroluminescence spectra of the device were measured with a Keithley 236 meter, an IL 1400A light meter and a photo-multiplier tube. All device measurements took place at room temperature under ambient conditions.

3. Results and discussion

3.1. Synthesis

The synthetic pathway for the monomers, their respective homopolymers and their copolymers is shown in Scheme 1. The two vinyl monomers prepared were the hole-transporting *N*-(4-methoxyphenyl)-*N*-(4-vinylphenyl)naphthalen-1-amine (vMeONPA) and the hole-blocking 2-phenyl-5-(4-vinylphenyl)-1,3,4-oxadiazole (vOXA). Unlike similar charge transporting vinyl monomer prepared using addition reaction, the vinyl monomers presented here were derivatized directly onto their respective charge transporting moieties and therefore with high yield and purity. The hole-transporting vMeONPA was synthesized in three reaction steps. It began with a modified Ullmann condensation to produce the arylamine *N*-(methoxyphenyl)-*N*-phenyl-1-naphthylamine (MeONPA), followed by a Vilsmeyer formylation step for the aldehyde derivative *N*-(methoxyphenyl)-*N*-4-formalphenyl-1-naphthylamine (MeONPA-CHO), and then a Wittig coupling reaction to produce the vinyl monomer vMeONPA [7,8]. The 4-(5-phenyl-1,3,4-oxadiazol-2-yl)benzaldehyde derivative (OXA-CHO) was synthesized directly from a ring-closure reaction between 4-formylbenzoyl chloride and 5-phenyl-2*H*-tetrazole with reasonable good yield as well. The aldehyde OXA-CHO then reacted with methyl triphenyl phosphonium via a Wittig coupling reaction to yield the hole-blocking vinyl monomer vOXA.

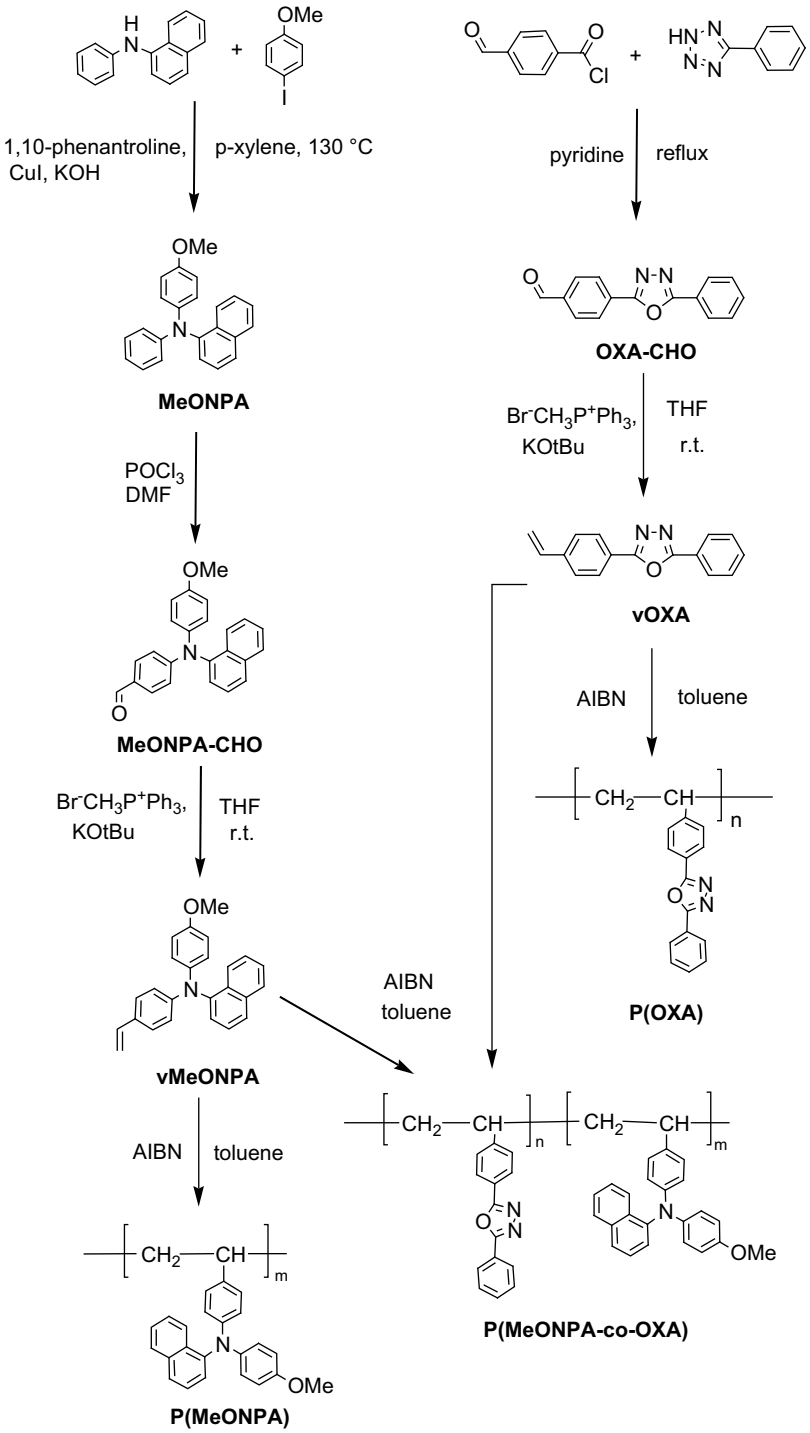

Scheme 1. Synthetic routes for the vinyl monomers, homopolymers and copolymers.

Copolymerization of the two vinyl monomers was conducted in an oxygen-free environment prepared from repeated nitrogen purging and freeze–thaw degassing cycles. Copolymerization was achieved by a free-radical solution polymerization using AIBN as the initiator and at different monomers molar feed ratios (F_1, F_2, see Table 1). Composition of the copolymers was determined from the aromatic/aliphatic intensity peak ratios using their ^{1}H NMR spectra. The experimentally determined composition and the molecular weight of the homopolymers (P(MeONPA), P(OXA)) and the copolymers at different feed ratios are given in Table 1. The results indicated vOXA has higher reactivity then vMeONPA as the resulting copolymers contained higher OXA composition then their feed ratios. The homopolymer P(OXA) also has higher MW than the rest. This could be due to planar OXA also has smaller steric hindrance compared to the non-planar and bulkier MeONPA monomer. In general, polydispersity index (PDI) for the polymers is relatively high, as compared to the most probable distribution value (PDI = 2, for $p = 1$), and could have been caused by chain transfer reaction to non-reactive small MW species and to an extent contributed by the relatively high monomer concentration employed in the polymerization process.

Table 1
Composition and MW of P(MeONPA), P(OXA) and P(MeONPA-co-OXA).

MeONPA (feed, F_1)	OXA (feed, F_2)	MeONPA[a] (mol%)	OXA[a] (mol%)	MeONPA[a] (wt%)	OXA[a] (wt%)	Yield (%)	M_n[b]	M_w[b]	PDI[b]
100	0	100	0	100	0	98	27,000	60,000	2.2
95	5	93	7	95	5	85	25,000	50,000	2.0
85	15	82	18	87	13	80	30,000	87,000	2.9
70	30	69	31	76	24	65	31,000	84,000	2.7
50	50	47	53	56	44	75	40,000	96,000	2.4
30	70	26	74	33	67	56	24,000	69,000	2.9
0	100	0	100	0	100	97	80,000	168,000	2.0

[a] The copolymer composition was determined by integration of ^{1}H NMR peak area.
[b] The weight-average (M_w) and number-average (M_n) molecular weights were determined by GPC using poly(styrene) MW standard in THF. Conditions: wavelength 254 nm (detector), flow rate 1 mL/min, mobile phase THF.

3.2. Thermal properties

The thermal properties of the homopolymers and the copolymers were measured by thermal gravimetric analysis (TGA) and differential scanning calorimetry (DSC) all under nitrogen atmosphere. DSC thermograms for the homopolymers and the copolymers are shown in Fig. 1. A single T_g and comparable heat capacity increment at the T_g (ΔC_p) indicated the copolymers are homogeneous and do not contain mesophase separated segmental structures. The glass transition temperature ($T_{g\ midpoint}$) of P(MeONPA) and P(OXA) were 132 and 187 °C respectively. We have previously reported $T_{g\ midpoint}$ as high as 161 °C was obtained for the non-substituted P(H-NPA) [24], but the methoxy labeling enable us to identify and to calculate the composition easily using either FT-IR or ^{1}H NMR. There was no melting or re-crystallization detected for scanning temperature up to 250 °C indicating both the homopolymer and the copolymers were amorphous in nature. By comparison, the melting points (T_m) of the model compound MeONPA and diphenyl-1,3,4-oxadiazole were 110 and 138 °C respectively.

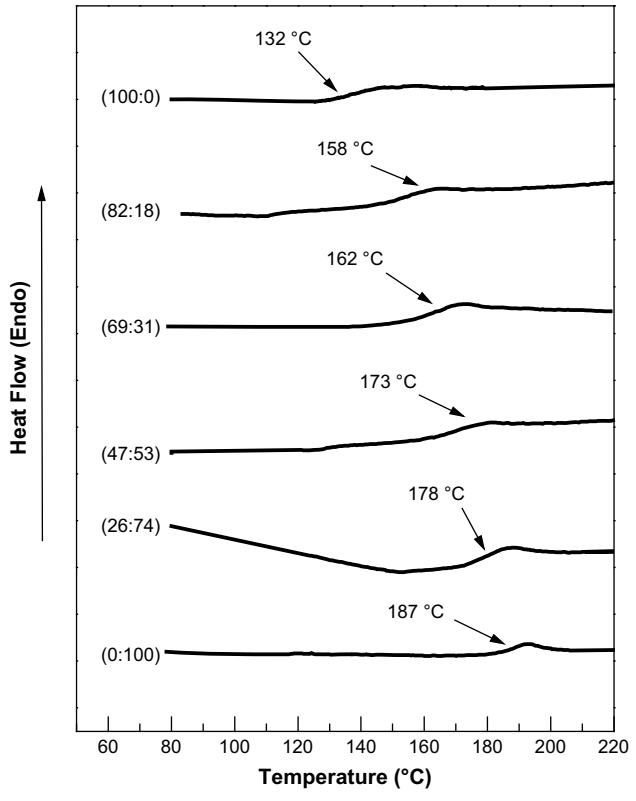

Fig. 1. DSC thermograms for P(MeONPA), P(OXA) and P(MeONPA-co-OXA) at different composition ratios (given in bracket).

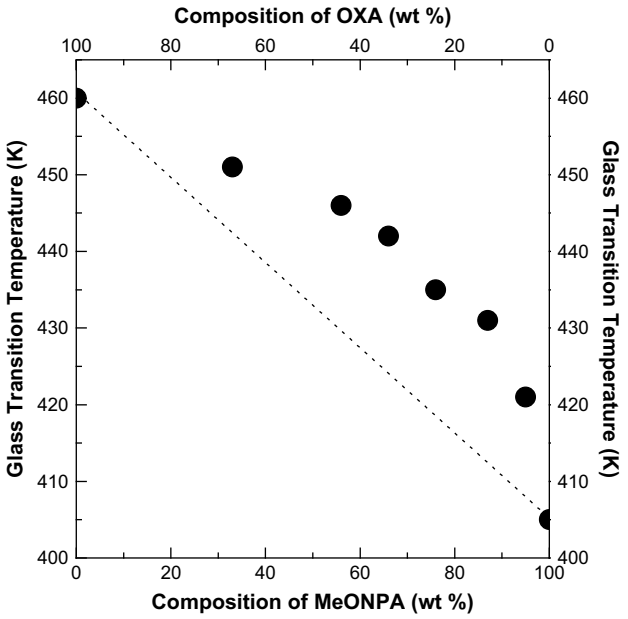

Fig. 2. Variation of T_g with copolymer composition for P(MeONPA-co-OXA). Experimental data are shown as solid circles; theoretical calculation according to the Fox equation shown in dashed line.

Glass transition temperature dependence on composition for copolymers without specific interaction has been described by the Fox equation [28]:

$$1/T_g = w_1/T_{g1} + w_2/T_{g2}$$

in which w_1 and w_2 are the weight fractions of repeating unit for monomers 1 and 2 respectively, and T_{g1} and T_{g2} are the glass transition temperatures of the homopolymer for monomers 1 and 2 respectively. Fig. 2 shown the experimentally observed T_g deviated from the arithmetic mean values as predicted by the Fox equation. A substantial positive deviation was observed indicating a favorable positive interaction between the electron-rich MeONPA and electron-deficient OXA monomer pair. A small but discernible red-shift in the photoluminescence spectra and a small variation in the redox values in following cyclic voltammetry studies on the copolymers (to discuss later) coincided with the results given here. The onset degradation temperature of the homopolymers and copolymers from TGA was in the range 317–421 °C. It was found that copolymers with higher MeONPA contents in general have better thermal stability than those with higher OXA contents. The results of the thermal analyses are summarized in Table 2.

Table 2
Thermal properties of P(MeONPA), P(OXA) and P(MeONPA-co-OXA).

Polymers	T_d[a] (°C)	Weigh lost (%)	T_g[b] (°C)	ΔC_p (J/(g °C))
P(MeO-NPA)	421	75	132	0.21
P(MeONPA-co-OXA 93:7)	393	65	148	0.17
P(MeONPA-co-OXA 82:18)	398	80	158	0.18
P(MeONPA-co-OXA 69:31)	378	72	162	0.18
P(MeONPA-co-OXA 47:53)	339	79	173	0.19
P(MeONPA-co-OXA 26:74)	318	72	178	0.16
P(OXA)	317	85	187	0.20

[a] Measured by TGA under nitrogen purge at a heating rate: 20 °C/min.
[b] Measured by DSC under nitrogen purge at a heating rate: 20 °C/min.

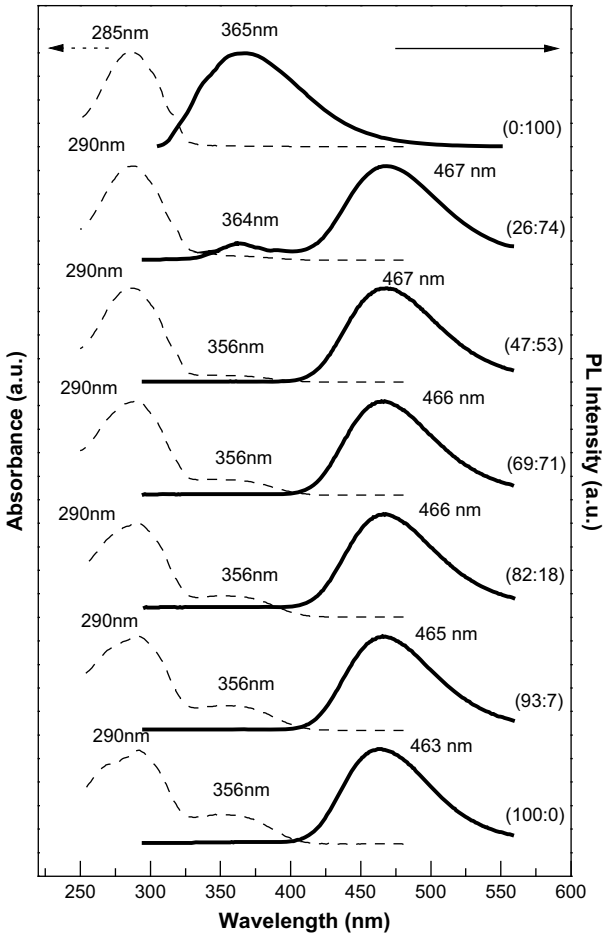

Fig. 3. Optical absorption (dashed-lines) and photoluminescent spectra (solid lines) of P(MeONPA), P(OXA) and P(MeONPA-co-OXA) at different MeONPA:OXA mole ratios.

3.3. Optical absorption and photoluminescence

The absorption and photoluminescence spectra of the polymers were measured in dichloromethane. In general, the conductive vinyl polymers and their copolymers were optically clear and do not absorbed significantly in the visible region due to lack of long range pi electron delocalization. P(OXA) emitted only in the UV region ($\lambda_{max} = 365$ nm) while P(MeONPA) has a blue emission ($\lambda_{max} = 463$ nm). According to Fig. 3, the photoluminescence spectrum of P(OXA) overlapped significantly with the absorption spectrum of P(MeONPA) indicating possibility of energy transfer from P(OXA) to P(MeONPA). For copolymers with higher MeONPA contents, only a blue emission was detected suggesting emission by OXA has been absorbed by MeONPA units completely. Only for copolymer with very higher OXA contents (74% OXA or above), two distinct emission maxima relating to OXA and MeONPA were detected. Moreover, emission spectra of the copolymers were slightly red-shifted (2–4 nm) compared to that of P(MeONPA). The result can be attributed to interaction between the electron-deficient OXA (acceptor) and electron-rich MeONPA (donor) units. A summary for the optical properties are given in Table 3.

Table 3
Optical properties of P(MeONPA), P(OXA) and P(MeONPA-co-OXA).

Polymers	λ_{max} absorption (nm)	λ_{max} emission (nm)
P(MeO-NPA)	290, 356	463
P(MeONPA-co-OXA 93:7)	290, 356	465
P(MeONPA-co-OXA 82:18)	290, 356	466
P(MeONPA-co-OXA 69:31)	290, 356	466
P(MeONPA-co-OXA 47:53)	290, 356	467
P(MeONPA-co-OXA 26:74)	290, 356	467, 364
P(OXA)	285	365

The photoluminescence and optical absorption spectra of the homopolymers and copolymers were measured in dilute dichloromethane solution (1×10^{-6} M).

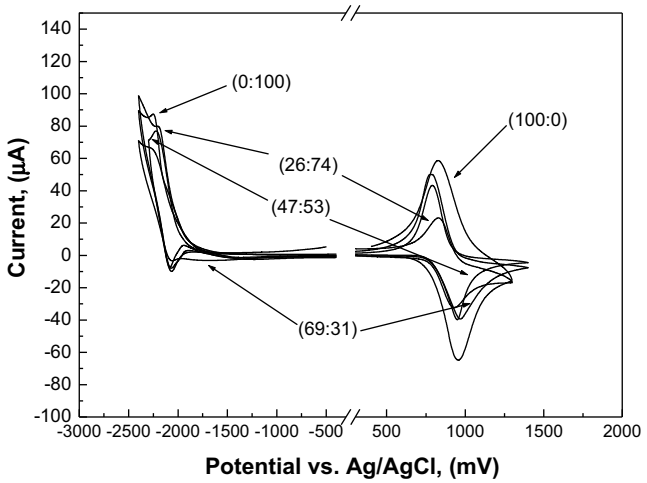

Fig. 4. Cyclic voltammograms of P(MeONPA-co-OXA) thin-film cast on Pt working electrode at different MeONPA:OXA monomer ratios. Experimental conditions: Pt working and counter electrodes; Ag/AgCl reference electrode; ACN/TBAHFP 0.1 M, scan rate 200 mV/s.

3.4. Electrochemical properties

The electrochemical properties of the homopolymers, P(MeONPA) and P(OXA), and their copolymers in solid thin-film form (cast on Pt working electrode) were studied by cyclic voltammetry (see Fig. 4). In Fig. 5, a pair of reversible anodic oxidation wave with the half-wave potential at 0.89 V (vs. Ag/AgCl) was detected for P(MeONPA). The highest occupied molecular orbital (HOMO, −5.23 eV) was determined from the oxidation potential with respect to Fc: HOMO = $E^{ox}_{1/2}$ vs. Fc + 4.8 V [29,30]. The LUMO (lowest unoccupied molecular orbital, −2.14 eV) was found by subtracting the band-gap energy (determined from UV absorption edge) from the

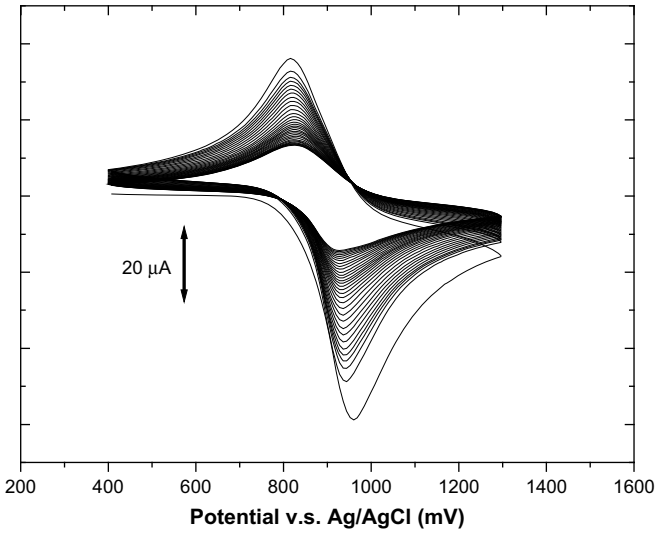

Fig. 5. Cyclic voltammogram of P(MeONPA) thin-film cast on the Pt working electrode. Conditions: Pt working and counter electrodes; Ag/AgCl reference electrode; ACN/TBAHFP 0.1 M, scan rate 500 mV/s.

Table 4
Electrochemical properties of P(MeONPA), P(OXA) and P(MeONPA-co-OXA).

Polymers	E_{ox} vs. Ag/AgCl[a] (mV)	E_{ox} vs. Fc (mV)	HOMO (eV)	E_{red} vs. Ag/AgCl (mV)	E_{red} vs. Fc (mV)	LUMO[c] (eV)
P(MeO-NPA)	0.87	0.43	5.23[b]	–	–	2.14[c]
P(MeONPA-co-OXA 93:7)	0.87	0.42	–	–	–	–
P(MeONPA-co-OXA 82:18)	0.87	0.44	–	2.14	2.58	–
P(MeONPA-co-OXA 69:31)	0.85	0.41	–	2.17	2.61	–
P(MeONPA-co-OXA 47:53)	0.84	0.40	–	2.15	2.59	–
P(MeONPA-co-OXA 26:74)	0.86	0.42	–	2.13	2.57	–
P(OXA)	–	–	6.04[c]	2.13	2.57	2.23[b]

[a] Oxidation potential relative to Ag/AgCl electrode.
[b] HOMOs/LUMOs were calculated assuming HOMO of Fc = 4.8 eV.
[c] LUMOs/HOMOs were calculated by subtracting the E_g from their respective HOMOs/LUMOs. Band-gap energies were determined from the UV absorption edge.

HOMO value. The results are similar to those previously measured using a polymer solution (HOMO = 5.15 eV, LUMO = 2.11 eV) [24]. The redox reversibility of P(MeONPA) is excellent, repeated anodic oxidations and reductions (after 64 cycles) did not change the peak shape as seen from the cyclic voltammogram given in Fig. 5. However, the voltammetric current became smaller during successive cycling due to dissolution of the polymer into the supporting electrolyte. For P(OXA), the LUMO (−2.23 eV) was calculated from the reduction potential vs. Fc: $E_{1/2}^{red}$ vs. Fc + 4.8 V [29,30]. As the oxidation potential of P(OXA) lied outside the scan range, its HOMO was calculated by adding the band-gap energy (determined from UV absorption edge) with the LUMO. The high ionization potential of OXA (HOMO = −6.04 eV), making it an effective hole-blocking unit, was induced by the electron-deficient oxadiazole ring [25]. As a result, the inclusion of hole-blocking OXA in the copolymers effectively limited the hole current in the copolymer-based HTL.

The redox properties of the copolymers were similar to that of the homopolymers, such as the half-wave oxidation and reduction (see Table 4). Only a slight variation in the values was detected, indicating the electrochemical properties of the OXA and MeONPA moieties do not interfere with each other significantly. As a result, we can conclude that the copolymers were oxidized via the MeONPA moieties and reduced via the oxidiazole moieties independently.

3.5. Electroluminescent device properties

3.5.1. Heterojunction HOLEDs

Tang et al. have demonstrated by confining the recombination of hole-electron pairs at the interface of the hole and electron-transporting layers, the emission efficiency of the device can increase drastically [1,2]. The multilayer device is known as heterojunction OLED. The multilayer small molecule-based OLEDs were fabricated using successive vacuum evaporation. In the followings, we fabricated the heterojunction devices using two different processes – solution spin coating for the hole-limiting copolymer layer and vacuum evaporation for the small molecule-based (AlQ_3) electron-transporting layer (Fig. 5).

Oxidative degradation of AlQ_3, a commonly used electron-transporting material and green emitter, is the main problem for AlQ_3-based OLEDs. A low work function calcium cathode (−2.9 eV) [31,32] can facilitate the injection of electrons into the AlQ_3 layer thus reduced the formation of unstable cationic species and led to better device stability [10]. In addition, a series of hole-limiting copolymers containing different ratios of hole-transporting (MeONPA) and hole-blocking (OXA) moieties were used as the HTL in this report. It was expected that at a certain copolymer composition, charge balance would be established. The properties of the devices were reported with an attempt to relate their performance with the copolymer composition. The configuration for the heterojunction OLEDs adopted was ITO/PEDOT:PSS/copolymer/AlQ_3/Ca/Al. The PEDOT:PSS (HOMO: −5.15 eV), a hole injection layer (HIL), was applied mainly to facilitate the injection of holes from the ITO anode (HOMO: −4.8 eV) to the organic hole-transporting layer. As a result, the onset or turn-on voltage for the diodes was lowered. A summary for the electroluminescent results is given in Table 5.

The luminance (cd/m^2) vs. current density (mA/cm^2) curves for the OLEDs at different copolymer compositions are shown in Fig. 6. According to Fig. 6, highest luminance was observed for the copolymer with 82/18 MeONPA/OXA mol ratio at 23,856 cd/m^2. It is suggested at this composition range, charge balance was achieved for the AlQ_3-based OLED. For copolymers with either a higher or lower OXA contents, lower luminance was detected under the same applied current density. Compared to a device employing the hole-transporting only homopolymer P(MeONPA), a maximum luminance of only 6608 cd/m^2 was resulted. It confirmed our speculation that higher hole current not necessary improved emission luminance but rather incited rapid degradation of the electron-transporting and emitting AlQ_3 instead. For the copolymers with OXA contents higher than 18 mol%, the decrease in luminance was due to diminishing of the hole current. It was also found that a higher turn-on voltage was required for the devices with higher OXA composition (see Table 5) and could be related to the low-lying HOMO for OXA (−6.04 eV) [33].

The current efficiency (cd/A) for the HOLED devices as a function of applied current density until failure is given in Fig. 7. The inset in Fig. 7 shown the dependence of luminance with copolymer composition at three different current densities (100, 200, 300 mA/cm^2). Disregard the current density, a maximum luminous can be found near 15–20 mol% OXA for the copolymers indicating an optimal composition existed. Examining in details of the current efficiency curves given in Fig. 7, two distinct degradation mechanisms at higher applied current density were found according to the gradient of the decreasing slope. For polymers (including the homopolymer P(MeONPA)) with less then 18 mol% OXA, an additional turning point (indicated by arrows in Fig. 7) in the decreasing slope was detected. The current efficiency decayed initially with a steep slope then followed by a second single exponential decay. The phenomenon has been observed previously and suggested relating to interface breakdown under high

Table 5
HOLED device properties with configuration of ITO/PEDOT:PSS/polymer/AlQ_3/Ca/Al. The polymers were P(MeONPA) and P(MeONPA-co-OXA).

Polymers	Turn-on voltage (V)	Max luminance (cd/m^2)	λ_{em} (nm)	Max current efficiency (cd/A)	Driving voltage at max luminance (V)	Current density at max device efficiency (mA/cm^2)
P(MeO-NPA)	8.5	6608	534	3.52	20.8	474
P(MeONPA-co-OXA 93:7)	9.0	9640	532	4.0	20.6	666
P(MeONPA-co-OXA 82:18)	9.2	23,856	532	4.2	17.8	1075
P(MeONPA-co-OXA 69:31)	10.2	14,756	534	3.49	18	715
P(MeONPA-co-OXA 47:53)	10.3	3668	528	1.89	21	314

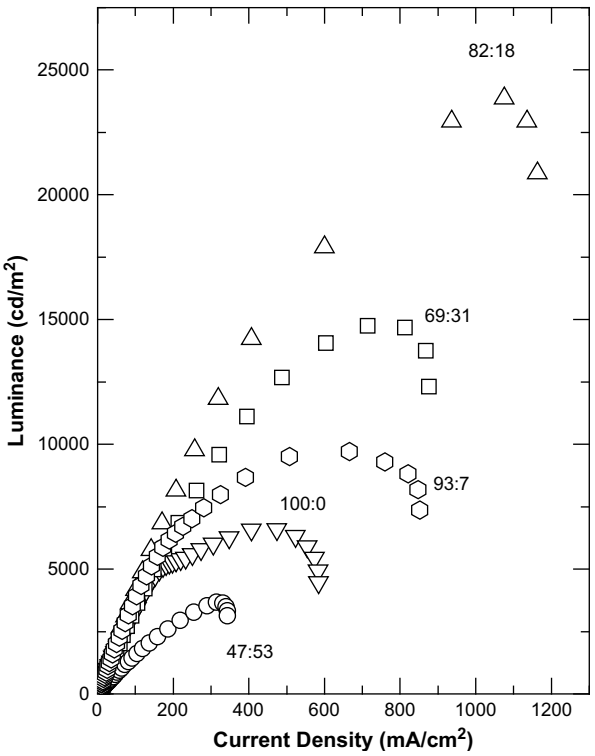

Fig. 6. Electroluminescent luminance (cd/m^2) vs. current density (mA/cm^2) of the HOLEDs with the configuration ITO/PEDOT:PSS/polymer/AlQ_3/Ca/Al. The polymers were P(MeONPA) and P(MeONPA-co-OXA) at different composition ratios.

operation current [11]. The same phenomenon, however, was not detected for OLEDs employing copolymers with higher OXA content indicating the multiple decaying slopes could be associated with the degradation of the AlQ_3 emitters. Although one can not distinguish specifically whether the steep decrease in current efficiency was related to the formation of non-emitting cationic AlQ_3^+ species or a reduction in electron current due to traps formation, it could be likely a combination of different causes. For copolymers with higher OXA contents (18 mol% and above), the initial steep exponential decay was not observed suggesting at higher OXA contents, reducing the hole current and therefore the possibility of holes leaking into the ETL contributed to the stability of the devices as a whole. In Fig. 7, the charge-balance device with the copolymer 82/18 MeONPA/OXA mol ratio, although the copolymer does not have the highest T_g, tolerated the maximum span in applied current density (ca 1200 mA/cm^2) before failure. The results against indicated the advantage of achieving charge-balance for a heterojunction OLED.

All the OLEDs shown typical green AlQ_3 emission except for the device employing P(MeONPA-co-OXA 47:53) as the HTL (see Fig. 8). A small blue emission shoulder (indicated by an arrow) associated with MeONPA was detected for this copolymer indicating some of the excessive electrons might have entered the HTL. The LUMO of OXA (−2.23 eV) is somewhat low-lying compared to MeONPA (−2.14 eV) and OXA is liable to accept electron releasing from AlQ_3. The formation of excitons in the HTL layer resulted in the blue emission associated with MeONPA for this device.

3.5.2. Hole current only devices

In order to verify the hole current was indeed limited by the inclusion of OXA moieties in the copolymers, a series of hole current only devices was prepared. The single layer devices have the configuration ITO/PEDOT:PSS/copolymer/Au. Again a hole-injecting PEDOT:PSS layer (HOMO −5.15 eV) was applied to facilitate the injection of holes into the organic layer (compared to HOMO for the hole conducting P(MeONPA) is −5.23 eV) as well as maintaining an ohmic contact. A high work function and electron blocking Au metal was used as the cathode instead. The working function for Au at −5.1 eV is much lower than the LUMO for the copolymers (from −2.14 to −2.23 eV), and as a result the large

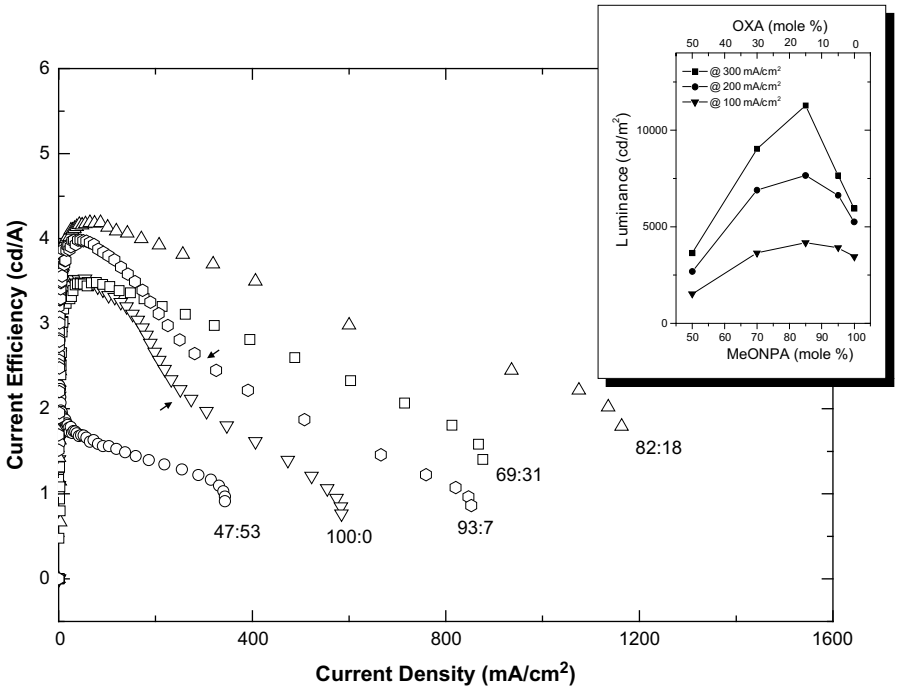

Fig. 7. Current efficiency (cd/A) vs. current density (mA/cm^2) of the HOLEDs over the full current density range until device failure. The polymers were P(MeONPA) and P(MeONPA-co-OXA) at different composition ratios. The arrows indicated the position of the inflexion points associated with AlQ_3 degradation for polymers with high hole current. The inset diagram shown variation of luminance with composition at three different current densities (100, 200, 300 mA/cm^2).

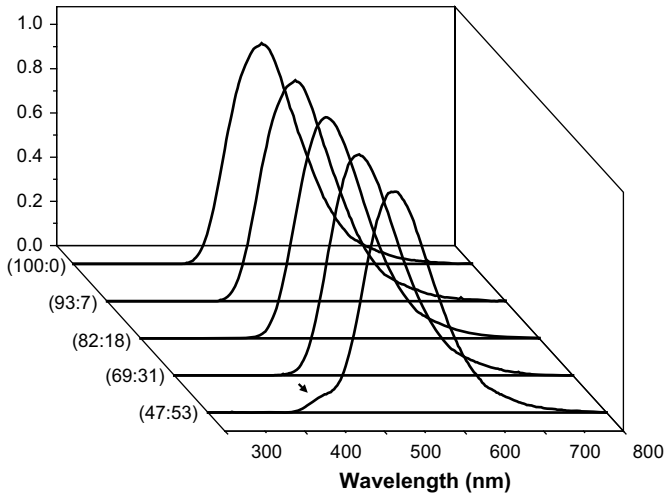

Fig. 8. The EL spectra of the HOLEDs. The polymers were P(MeONPA) and P(MeONPA-co-OXA) at different composition ratios. The arrow indicated the extra blue emission related to MeONPA.

energy barrier deterred the injection of electrons from the cathode. Thus the currents measured and shown in Fig. 9 are largely hole current only. The current density vs. voltage (log I vs. V) for three such "hole current only" devices is given in Fig. 9 [34,35]. The results indicated the current measured decreased in proportion to an increase of OXA contents in the copolymers. Similar results have been observed for a series of carbazole/oxadiazole vinyl copolymers prepared by Jiang et al. [28]. A reduce in hole transport ability with increased OXA was suggested to be the result of reduction in hopping sites. The decrease in hole current was found also not only related to an increase in the OXA composition but also to their dispersion in the polymer matrix. A continuous decrease in hole current with an increase in OXA contents for our devices indicated random or statistical distribution of the OXA moieties in the copolymers. In an dark injection space-charge-limited-current (DI-SCLC) experiment measuring the I–V characteristics for a series of hole-transporting small molecules with similar device configuration (except Ag was used as the cathode) [33], the PEDOT:PSS HIL was found to be effective in forming an ohmic or quasi-ohmic contact with the organic

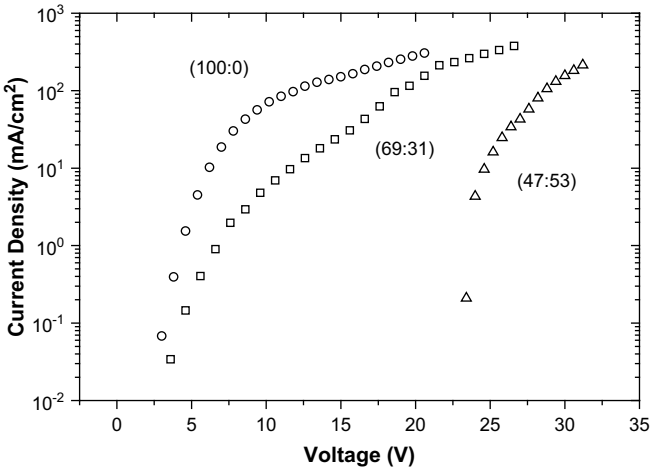

Fig. 9. Current density (mA/cm^2) vs. voltage (V) for the "hole current only" devices with the configuration ITO/PEDOT:PSS/polymer/Au. The polymers were P(MeONPA) and P(MeONPA-co-OXA 69:31 and 47:53).

layer with low hole mobility. At the limit of high electric field (>100 kV/cm), the conduction was trap free and space-charge-limited-current was dominated by the bulk conduction of holes only. Similarly, it has also been proposed for an injection energy barrier height less than 0.3 eV, the metal/organic interface can be treated as ohmic and capable of supplying the bulk with space-charged-limited-current [36].

4. Conclusion

In this study, the synthesis of two vinyl monomers including a hole-transporting *N*-(4-methoxyphenyl)-*N*-(4-vinylphenyl)naphthalen-1-amine (vMeONPA) and a hole-blocking 2-phenyl-5-(4-vinylphenyl)-1,3,4-oxadiazole (vOXA) was presented. The synthetic routes were specific, facile, and with high yield. A series of copolymers with different MeONPA/OXA compositions and thus different charge transporting properties were prepared using solution free-radical polyaddition polymerization. The vinyl copolymers have high MW and T_g yet were soluble in most common organic solvents. The hole current for the copolymers was verified to decrease with an increase in OXA contents using "hole current only" devices. Heterojunction OLEDs fabricated using the "hole-limiting" copolymers as the HTL whereas the commonly used AlQ_3 as the ETL were studied. At the optimum MeONPA/OXA composition (82/18 mol ratio), the hole current limited HTL effectively produced a charge-balance device with outstanding performance (4.2 cd/A and ca 24,000 cd/m^2). The results indicated the charge hopping process between MeONPA moieties can be effectively blocked by the presence of OXA moieties [37]. Improvement in stability of the charge-balance device can be shown from the current efficiency vs. current density curves (see Fig. 7). Not only the charge-balance device tolerated up to ca 1200 mA/cm^2 before failure, the current efficiency also decrease with a single slower decreasing slope. AlQ_3 was used only as an example to illustrate the advantages of achieving charge-balance for such electroluminescent device. As the composition of the copolymer can be tailored easily by adjusting the monomer feed ratio, the transport properties can be easily matched with other ETL or emitters as well. The hole-limiting copolymers are bipolar in nature, vinyl monomer with different emission characteristic can be copolymerized to produce homojunction POLEDs with improved efficiency at different hue will be a subject following.

Acknowledgment

The authors would like to acknowledge the support of this research by the University Grant Council (UGC) of Hong Kong (grant# HKBU/2013/05P). T-H Lee would like to thank Mr. Lau Chung Yin for his assistance on the electrochemical measurements. L. Leung would also like to acknowledge helps and discussion on device properties provided by Prof S.K. So at the Dept. of Physics at HKBU.

References

[1] Tang CW, VanSyke SA. Appl Phys Lett 1987;51:913.
[2] Tang CW, VanSyke SA. J Appl Phys 1989;65:3610.
[3] Higginson KA, Zhang XM, Papadimitrakopoulos F. Chem Mater 1998;10:1017.
[4] Hamada Y. IEEE Trans Electron Device 1998;363:327.
[5] Malliaras GG, Shen Y, Dunlap DH, Murate H, Kafafi ZH. Appl Phys Lett 2001;79:2552.
[6] Popovic ZD, Aziz H, Hu NX, Hor AM, Xu G. Synth Met 2000;111–112:229.
[7] Young RH, Tang CW, Marchetti AP. Appl Phys Lett 2002;80:874.
[8] Popovic ZD, Aziz H, Ioannidis A, Hu NX, dos Anjos PNM. Synth Met 2001;123:179.
[9] Popovic ZD, Aziz H, Hu NX, dos Anjos PNM. Appl Phys Lett 2001;89:4673.
[10] Aziz H, Popovic ZD, Hu NX, Hor AM, Xu G. Science 1999;283:5409.

[11] Ni SY, Wang XR, Wu YZ, Chen HY, Zhu WQ, Jiang XY, et al. Appl Phys Lett 2004;85:878.
[12] Zhang ZL, Jiang XY, Xu SH, Nagatomo T, Omoto O. Synth Met 1997;91:131.
[13] Papadimitrakopoulos F, Mathai MK, Hsieh BR. J Appl Phys 2004;95:8240.
[14] Van Slyke SA, Chen CH, Tang CW. Appl Phys Lett 1996;69:2160.
[15] Abkowitz MA, Forsythe EW, Gao Y. J Phys Chem B 2000;104:3948.
[16] Rieβ W, Vestweber H. Synth Met 1997;91:181.
[17] Li J, Ma C, Tang J, Lee CS, Lee S. Chem Mater 2005;17:615.
[18] Justin Thomas KR, Lin JT, Tao Y-T, Chien CH. Chem Mater 2002;14:2796.
[19] Justin Thomas KR, Lin JT, Tao Y-T, Chien CH. Chem Mater 2002;14:3852.
[20] Justin Thomas KR, Lin JT, Tao Y-T, Chien CH. J Mater Chem 2002;12:3516.
[21] Justin Thomas KR, Lin JT, Tao Y-T, Chien CH. Chem Mater 2004;16:5437.
[22] (a) Dailey S, Feast WJ, Peace RJ, Sage IC, Till S, Wood EL. J Mater Chem 2001;11:2238;
(b) Mutaguchi D, Okumoto K, Ohsedo Y, Moriwaki K, Shirota Y. Org Electron 2003;4:49;
(c) Suzuki M, Tokito S, Sato F, Igarashi T, Kondo K, Koyama T, et al. Appl Phys Lett 2005;86:103507.
[23] Tong KL, So SK, Ng HF, Leung LM, Yeung MY, Lo CF. Synth Met 2004;147:199.
[24] Lee TH, Tong KL, So SK, Leung LM. Jpn J Appl Phys 2005;1B(44):543.
[25] Brocks G, Tol A. J Chem Phys 1997;106:6418.
[26] Kim Y, Bae KH, Jeong YY, Choi DK. Chem Mater 2004;16:5051.
[27] Kim Y, Han K, Ha CS. Macromolecules 2002;35:8759.
[28] Jiang XZ, Register RA, Killeen KA, Thompson ME, Pschemitzka F, Sturm JC. Chem Mater 2000;12:2542.
[29] Thelakkat M, Schmidt HW. Adv Mater 1998;10:219.
[30] Kawamoto M, Mochizuki H, Tsutsumi O, Lkeda T, Lee B, Shirota Y. J Phys Chem B 2003;107:4887.
[31] Matsumura M, Jinde Y. Synth Met 1997;91:197.
[32] Hung LS, Lee ST. Mater Sci Eng 2001;B85:104.
[33] Tse SC, Tsang SW, So SK. J Appl Phys 2006;100:063708.
[34] van Woudenbergh T, Blom PWM, Huiberts JN. Appl Phys Lett 2003;82:985.
[35] Hulea IN, van der Scheer RFJ, Brom HB, Langeveld-Voss BMW, van Dijken A, Brunner K. Appl Phys Lett 2003;83:1246.
[36] Malliaras GG, Scott JC. J Appl Phys 1999;85:7246.
[37] Schein LB, Peled A, Glatz D. J Appl Phys 1989;66:686.